Journal of Molecular Cell Biology (2024), 16(1), mjae003 https://doi.org/10.1093/jmcb/mjae003
Published online January 22, 2024

Article

Rbfox1 controls alternative splicing of focal adhesion genes in cardiac muscle cells

Peter Zorn[1,†], Jaime Calvo Sánchez[1,†], Tala Alakhras[1], Barbara Schreier[2], Michael Gekle[2], Stefan Hüttelmaier[3], and Marcel Köhn[1,*]

[1] Junior Group 'Non-coding RNAs and RBPs in Human Diseases', Medical Faculty, University of Halle–Wittenberg, 06120 Halle (Saale), Germany
[2] Julius Bernstein Institute of Physiology, Medical Faculty, University of Halle–Wittenberg, 06112 Halle (Saale), Germany
[3] Institute of Molecular Medicine, Medical Faculty, University of Halle–Wittenberg, 06120 Halle (Saale), Germany
[†] These authors contributed equally to this work.
[*] Correspondence to: Marcel Köhn, E-mail: marcel.koehn@medizin.uni-halle.de

Edited by Zefeng Wang

Alternative splicing is one of the major cellular processes that determine the tissue-specific expression of protein variants. However, it remains challenging to identify physiologically relevant and tissue-selective proteins that are generated by alternative splicing. Hence, we investigated the target spectrum of the splicing factor Rbfox1 in the cardiac muscle context in more detail. By using a combination of *in silico* target prediction and in-cell validation, we identified several focal adhesion proteins as alternative splicing targets of Rbfox1. We focused on the alternative splicing patterns of vinculin (metavinculin isoform) and paxillin (extended paxillin isoform) and identified both as potential Rbfox1 targets. Minigene analyses suggested that both isoforms are promoted by Rbfox1 due to binding in the introns. Focal adhesions play an important role in the cardiac muscle context, since they mainly influence cell shape, cytoskeletal organization, and cell–matrix association. Our data confirmed that depletion of Rbfox1 changed cardiomyoblast morphology, cytoskeletal organization, and multinuclearity after differentiation, which might be due to changes in alternative splicing of focal adhesion proteins. Hence, our results indicate that Rbfox1 promotes alternative splicing of focal adhesion genes in cardiac muscle cells, which might contribute to heart disease progression, where downregulation of Rbfox1 is frequently observed.

Keywords: Rbfox1, alternative splicing, focal adhesion, cardiac muscle cells

Introduction

Alternative splicing is one of the fundamental posttranscriptional processes in eukaryotes that lead to the formation of protein variants originating from a single gene. This process critically relies on the inclusion or exclusion of exons, which is controlled by the binding of *trans*-acting splicing factors to pre-mRNAs. Consequently, alternative splicing contributes to an extensive repertoire of RNA and protein products that are functionally coordinated to regulate developmental stages in highly specialized tissues such as the brain, heart, and skeletal muscle (Pedrotti et al., 2015; Baralle and Giudice, 2017; Weyn-Vanhentenryck et al., 2018). For instance, PTBP1 and NOVA2 splicing factors are directly involved in regulating essential splicing events implicated in neuronal cell differentiation and migration, respectively (Boutz et al., 2007; Zhang et al., 2010). Moreover, aberrant splicing patterns can cause severe cellular defects that may result in pathological conditions in muscle tissues. In myotonic dystrophy 1 (DM1), for instance, reduced activity of the co-acting splicing factors MBNL1 and RBFOX1 is observed. Consequently, it was reported that several target mRNAs (mainly cytoskeletal and ion channel genes) produce aberrant splicing variants in DM1 tissues (Klinck et al., 2014).

An important group of splicing factors is the Rbfox protein family (Rbfox1, Rbfox2, and Rbfox3), which plays a pivotal role in tissue-specific alternative splicing regulation. These proteins are especially important for heart and skeletal muscle development as well as function (Conboy, 2017). Rbfox1 is a versatile RNA-binding protein that mainly binds to intronic (U)GCAUG elements adjacent to tissue-specific alternative exons but can also bind to 3′ untranslated regions of mRNAs

Received April 5, 2023. Revised November 30, 2023. Accepted January 19, 2024.

and pre-miRNAs (Jin et al., 2003; Lambert et al., 2014). It is assumed that Rbfox1 motifs in the downstream intron enhance the inclusion of the proximal exon cassette, while upstream motifs tend to promote exon skipping (Minovitsky et al., 2005; Zhang et al., 2008). The Rbfox1 gene shows a multitude of alternatively spliced exons that encode brain- and muscle-specific isoforms (Nakahata and Kawamoto, 2005; Damianov and Black, 2010). This is also reflected by the results of a recent study showing that tissue-specific regulation of alternative splicing is common in neuronal and muscle tissues (Tapial et al., 2017). Interestingly, alternative splicing within the Rbfox1 gene can also produce variants that change the inclusion of the nuclear localization signal, which ultimately affects cellular localization of the Rbfox1 protein (Kuroyanagi, 2009). Genome-wide profiling of alternative splicing revealed that loss of Rbfox1 *in vivo* leads to altered splicing events that cause progressive cardiac contractile dysfunction and heart failure (Frese et al., 2015). Notably, a muscle-specific isoform of Rbfox1 emerged prominently in cardiomyocytes during hypertrophy and heart failure even though Rbfox1 expression was considerably diminished in pathological human and mouse hearts. Moreover, global mRNA splicing in cardiomyocytes was directly affected by Rbfox1 depletion (Gao et al., 2016).

It is well established that focal adhesions constitute a crucial factor in sustaining proper cardiomyocyte function, and aberrant assembly of its components can contribute to heart failure (Samarel, 2014). In zebrafish models, the cell–matrix interactions mediated by focal adhesions are critically important for heart valve development and cardiac contractility (Hirth et al., 2016; Gunawan et al., 2019). Several muscle-specific components, such as metavinculin (mVcl) and alpha-actinin (Actn1), were identified, and their function in supporting cytoskeletal muscle cell properties has been revealed (Jin et al., 2003; Kanoldt et al., 2020). However, it is not yet entirely clear how alternative splicing of relevant muscle-specific variants is controlled and how this contributes to cellular phenotypes associated with muscle cell pathologies. In line with this, we aimed to investigate the target spectrum of Rbfox1 in more detail to evaluate whether detectable Rbfox1-promoted protein isoforms can confer tissue-specific cell properties.

Results

Identification of Rbfox1 as a splicing regulator of focal adhesion genes

To elucidate the contribution of Rbfox1 in heart pathologies, the expression levels of Rbfox1 mRNA were analyzed with publicly available RNA-seq datasets from knockout of EGFR (EGFR-KO), myocardial infarction (MI), and transverse aortic constriction (TAC) mouse models of cardiac dysfunction (Figure 1A; Schreier et al., 2013; Duan et al., 2017; Binas et al., 2020; GSE96561). In all three models, where normal heart function was compromised, a significant downregulation of Rbfox1 levels was observed, as described previously in other *in vivo* models (Figure 1A; Park et al., 2011; Frese et al., 2015). In contrast, Rbfox2 expression was unaltered in these models (Supplementary Figure S1A). Then, we aimed to identify the potentially involved Rbfox1 splicing targets. Rbfox1 is known to bind to its target RNAs predominantly in intronic regions. However, it was previously reported that Rbfox1-binding sites within one intron might have synergistic effects on alternative splicing (Conboy, 2017). Hence, we used an *in silico* approach to analyze how often the canonical Rbfox1-binding site *GCATG* is present in intronic regions of the mouse genome and the transcripts expressed in the heart (Figure 1B). Our results revealed that a large proportion of genes indeed contain multiple introns with several potential Rbfox1-binding sites. Interestingly, the transcript with the highest occurrence rate of Rbfox1-binding sites is the Rbfox1 mRNA itself, which was shown to be subject to an autoregulatory splicing mechanism (Supplementary Table S2; Damianov and Black, 2010).

To elucidate potential Rbfox1-regulated pathways in the heart muscle context, we used the DAVID clustering tool (Sherman et al., 2022) to group functionally related genes (Figure 1B) with key biological roles. Notably, focal adhesion genes exhibited the highest correlation with potential Rbfox1-bound transcripts (Figure 1C). Out of the 51 factors in the focal adhesion cluster (Supplementary Table S2), 16 (31%) were reported to directly localize in focal adhesions (Figure 1D), among which paxillin (Pxn) and vinculin (Vcl) were not previously described to be regulated by Rbfox1. Therefore, we focused on these two potential targets and characterized their splicing regulation in more detail. H9C2 rat myoblasts were used as a cell line model, which can be differentiated into cells that more closely resemble a maturated skeletal muscle or cardiac muscle phenotype (Branco et al., 2015). Protein expression analyses revealed that upon differentiation of H9C2 cells, Rbfox1 levels were remarkably increased (Figure 1E). Both Pxn and Vcl showed, in addition to the main protein form, an additional protein variant under differentiation conditions. For Vcl, we expected that this variant might reflect the alternatively spliced mVcl (Siliciano and Craig, 1982; Kanoldt et al., 2020). However, the Pxn variant we detected did not match any of the characterized Pxn protein forms. Interestingly, transcript databases (Ensembl and NCBI) suggested the presence of an alternatively spliced Pxn variant resembling the actual molecular weight as we detected. In contrast to Pxn, the Pxn variant potentially contains four additional exons (large exon 7 and three smaller exons). Since the molecular weight of the Pxn protein (60.8 kDa) is almost doubled (116.3 kDa), we named this previously uncharacterized variant extended Pxn (ePxn). To verify that the predicted Rbfox1 targets are regulated by an alternative splicing mechanism, we performed real-time quantitative polymerase chain reaction (RT-qPCR) to specifically detect the alternatively expressed exons in 6 of the 16 putative target mRNAs (Figure 1D) and determined their % spliced-in (PSI) values (Figure 1F). The other mRNAs were either not expressed in H9C2 or did not have alternative variants described before. The PSI values of Actn1, Actn4 (two different events a and b), Ptk2 (also known as focal adhesion kinase, FAK), Vcl, and Pxn significantly increased upon differentiation, while that of Flnb did not significantly change. These results clearly indicate that mVcl

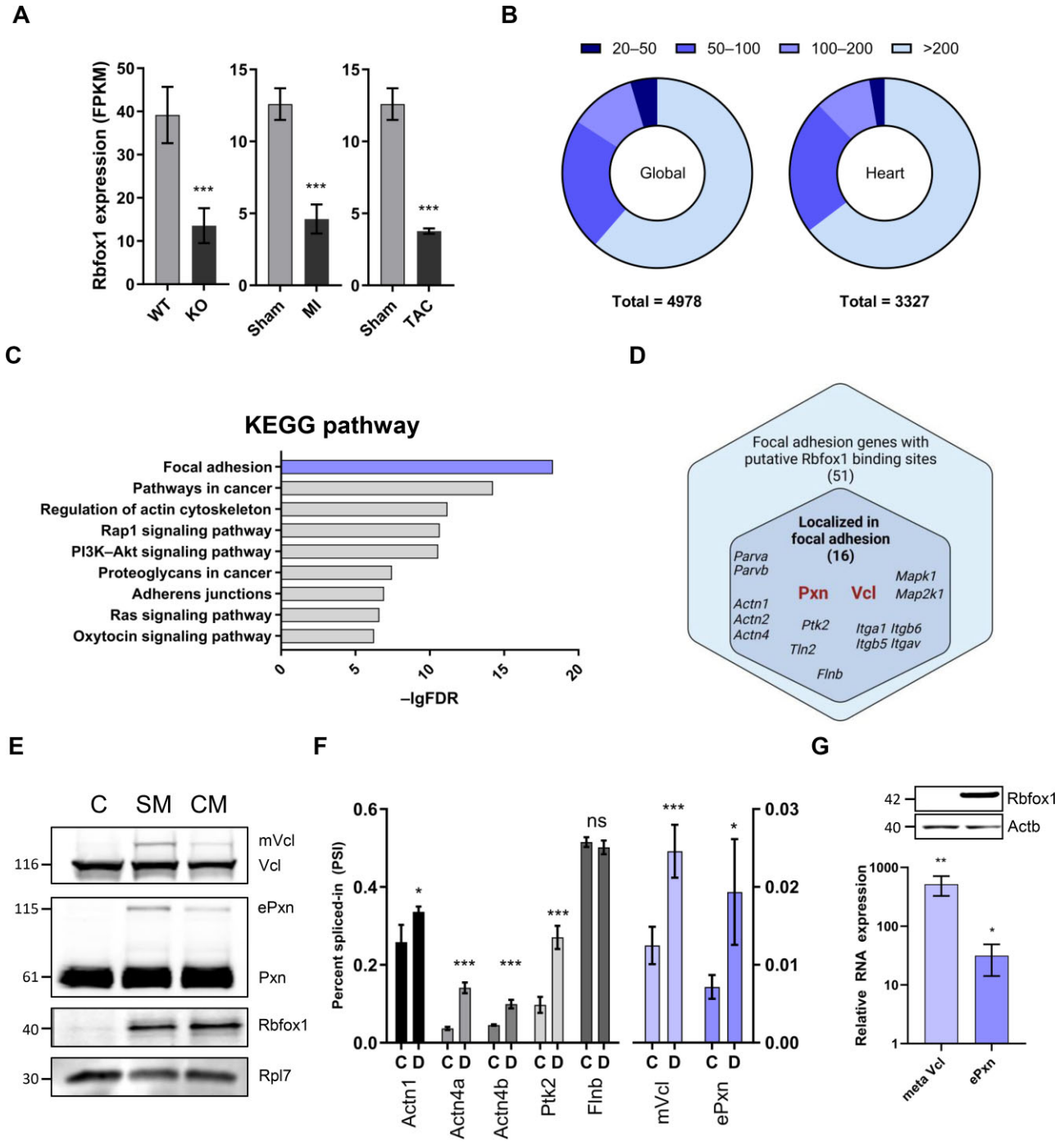

Figure 1 Rbfox1 controls alternative splicing of the focal adhesion genes Pxn and Vcl. (**A**) RNA expression levels of Rbfox1 in RNA-seq data from EGFR-KO, MI, and TAC mouse models. (**B**) *In silico* prediction of genes with >20 putative intronic Rbfox1-binding sites (*GCATG*) in the whole mouse genome (total number 4978) or specifically in mouse heart (total number 3327). These genes were classified into four categories with different color codings. (**C**) DAVID functional clustering of identified heart transcripts from **B**. FDR, false discovery rate. (**D**) Overlap of focal adhesion genes from the DAVID clustering and the gene ontology term 'Localized in focal adhesion'. (**E**) Western blot analysis of H9C2 cells with the indicated antibodies. Rpl7 was used as a loading control. C, undifferentiated cells; SM, skeletal muscle cells; CM, cardiac muscle cells. (**F**) RT-qPCR analysis for the indicated alternatively spliced mRNAs. The PSI value was calculated as the ratio of alternative variants to all variants under control (C) or differentiation (D) condition. For better visualization, the PSIs of mVcl and ePxn are shown with a different scaling. (**G**) RT-qPCR and representative western blot analysis of H9C2 cells after 48 h of transient overexpression of Rbfox1. Actb was used as a loading control. $n = 3$, significance determined by Student's *t*-test. ns, not significant; *$P < 0.05$; **$P < 0.01$; ***$P < 0.001$.

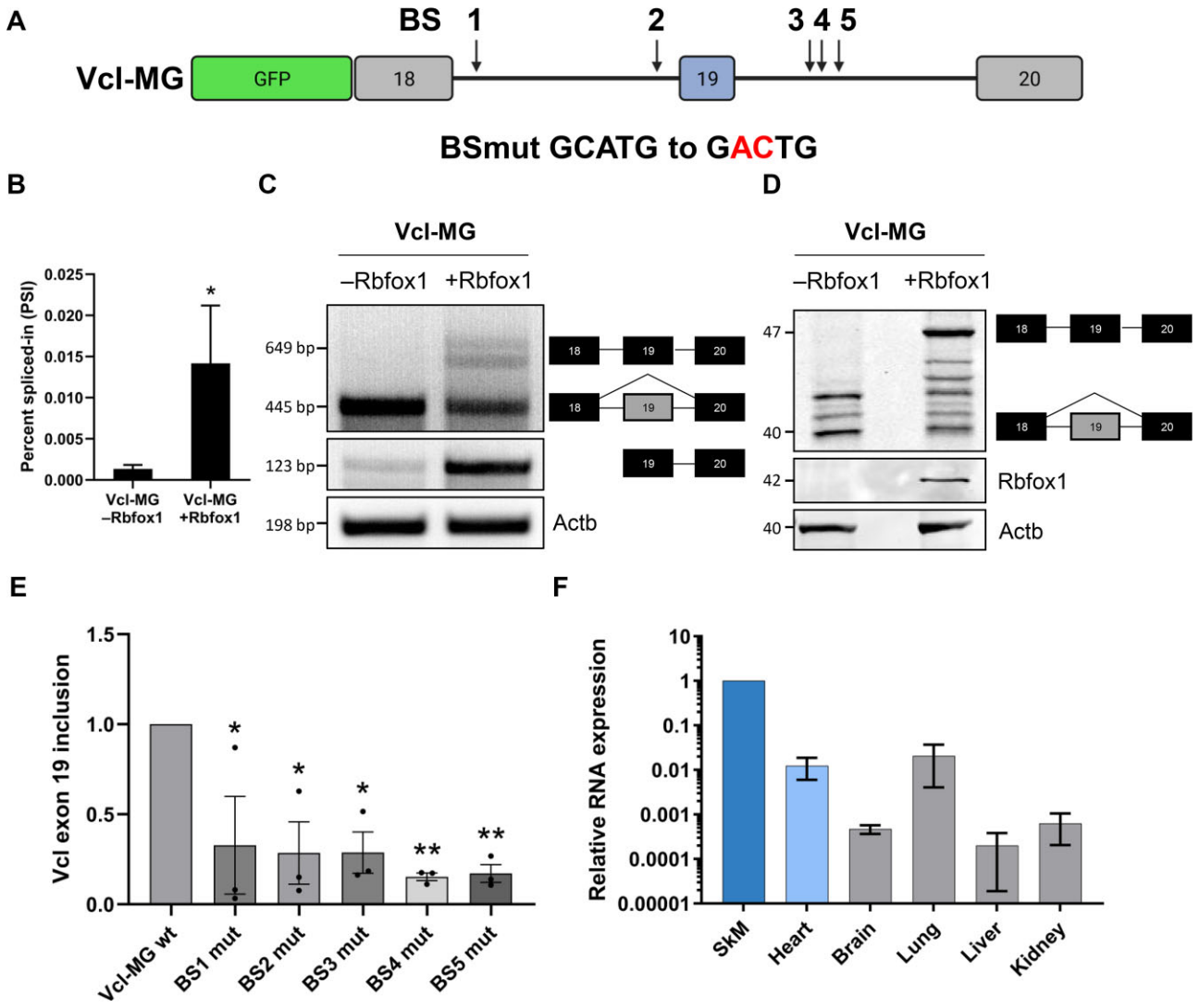

Figure 2 Characterization of the mVcl variant and analysis of the Rbfox1-dependent splicing. (**A**) Minigenes of Vcl were cloned as GFP fusion proteins with the exon–intron sequences as displayed; arrows indicate five putative Rbfox1-binding sites with a GCATG motif. For mutational analyses, individual GCATG motifs were mutated to GACTG. BS, Rbfox1-binding site. (**B**–**D**) Exon 19 inclusion in Vcl-MG upon Rbfox1 overexpression was analyzed by RT-qPCR (**B**), semi-quantitative PCR (**C**), and western blotting (**D**). Actb mRNA and Actb protein served as the loading control, respectively. (**E**) Exon 19 inclusion in wild-type Vcl-MG and mutant minigenes harboring single point mutation within the indicated putative Rbfox1-binding site upon Rbfox1 overexpression was determined by RT-qPCR. Shown are the fold changes relative to the wild-type minigene. (**F**) Relative mRNA expression levels of mVcl in various mouse tissues were determined by RT-qPCR. SkM, skeletal muscle. $n = 3$, significance determined by Student's *t*-test. *$P < 0.05$; **$P < 0.01$.

and ePxn are upregulated upon differentiation together with Rbfox1, implying an underlying alternative splicing mechanism. Subsequently, we performed overexpression experiments in undifferentiated H9C2 cells and observed a significant upregulation of mVcl and ePxn upon Rbfox1 overexpression (Figure 1G). Hence, we concluded that both alternative splicing events are likely to be regulated by Rbfox1 in differentiating cardiac myoblasts.

Rbfox1 controls mVcl splicing

We next sought to investigate how Rbfox1 controls splicing of Vcl to generate the alternative variant mVcl. The difference between Vcl and mVcl results from the internal addition of 68 amino acids (exon 19 of the Vcl gene) located at the C-terminal tail domain (Feramisco et al., 1982; Belkin et al., 1988). In the Vcl gene, we identified five putative Rbfox1-binding sites flanking the alternatively spliced exon 19, suggesting a potential regulation by Rbfox1. To test the role of Rbfox1 in mVcl splicing, we generated a set of minigene constructs as green fluorescent protein (GFP) fusion proteins. In addition to the wild-type minigene (Vcl-MG), we generated constructs that have point mutations (GCATG to GACTG) in individual Rbfox1-binding sites to inhibit Rbfox1-mediated regulation (Figure 2A). Upon transfection of the wild-type Vcl-MG construct together with

Rbfox1 overexpression plasmids in C2C12 mouse myoblasts, we detected a significant increase in exon 19 inclusion (Figure 2B). This result is consistent with the increase in endogenous mVcl mRNA upon Rbfox1 overexpression in H9C2 cells (Figure 1G) and again indicates that Rbfox1 promotes mVcl synthesis. The Rbfox1-dependent regulation of mVcl was further validated at the RNA and protein levels, respectively. Semi-quantitative PCR demonstrated the upregulation of exon inclusion (using exon 19-specific primers) and production of larger PCR products, indicating exon 19 inclusion (using primers spanning the flanking Vcl exons) in Rbfox1-overexpressing samples (Figure 2C). Western blotting revealed the production of a larger reporter protein exclusive to Rbfox1-overexpressing samples, again indicating the inclusion of the mVcl exon (Figure 2D). To identify the critical binding sites for Rbfox1, we compared the exon inclusion rates in five mutant minigene constructs and the wild-type minigene, and a significant decrease in Vcl exon 19 inclusion was detected in all tested point mutants (Figure 2E). These results suggest that Rbfox1 binds to multiple sites surrounding exon 19 and these sites could act in an additive manner.

Moreover, we analyzed RNA expression levels of mVcl (exon 19) across different mouse tissues and found the highest levels in the skeletal muscle and heart (Figure 2F), as previously shown by other studies (Maeda et al., 1997; Zemljic-Harpf et al., 2007). Intriguingly, mVcl expression level in lung tissue is also relatively high. This might be due to the well-known presence of mVcl in the smooth muscle of the respiratory system (Belkin et al., 1988; Amrani and Panettieri, 2003).

Alternative splicing of Pxn is controlled by Rbfox1

Pxn is known to contain multiple intrinsically disordered regions (IDRs) (Neerathilingam et al., 2016). As the ePxn variant has not been characterized thus far, we examined the putative structure of this isoform using AlphaFold (Jumper et al., 2021; Varadi et al., 2022). The predicted ePxn fold showed that the additional exons (highlighted in red) are also disordered (Supplementary Figure S1B). This insertion displays potential regulatory features, as it includes serine/threonine and tyrosine kinase motifs predicted using Human Protein Reference Database (HPRD) as well as three putative SH3-domain binding motifs of Src family kinases (Cestra et al., 1999). Thus, these findings imply a high regulatory potential of a region usually not present in Pxn, which could play key roles in controlling tissue-specific focal adhesion functions (Supplementary Figure S1C).

Rbfox1 is known to be an intronic splicing regulator that can promote exon inclusion. To investigate how Rbfox1 controls splicing of ePxn, different Pxn minigene constructs with wild-type (Pxn-MG) and mutated Rbfox1-binding sites flanking the alternatively spliced cassette (exon 7) were generated in fusion with GFP (Figure 3A). Then, we co-transfected Rbfox1 overexpression plasmids with Pxn-MG into C2C12 cells and determined the PSI value for exon 7 inclusion (Figure 3B) as well as the production of ePxn (Figure 3C and D). Rbfox1 overexpression resulted in a significant increase in exon 7 inclusion of Pxn-MG, thus providing additional evidence that Rbfox1 indeed regulates alternative splicing of Pxn (Figure 3B). Semi-quantitative PCR and western blotting confirmed that the exon cassette specific for ePxn is regulated by Rbfox1 (Figure 3C and D). Furthermore, Rbfox1-increased Pxn exon 7 inclusion was significantly reduced when using the Pxn-MG point mutants (BS2 mut, BS3 mut, and BS4 mut but not BS1 mut), indicating that Rbfox1 binds to multiple sites flanking exon 7 to facilitate alternative splicing and preferably regulates ePxn splicing via BS2 and BS3 (Figure 3E). In analogy to mVcl, ePxn showed the highest RNA expression levels in mouse skeletal muscle and heart (Figure 3F).

Since alternative splicing can strongly alter the amino acid composition of a protein and thus its function, we next analyzed cellular localization of Vcl and mVcl as well as Pxn and ePxn (Figure 4A) in H9C2 cells overexpressing GFP fusion proteins. As shown in Figure 4B, both Vcl and Pxn variants showed clearly defined localization in focal adhesion sites, by using endogenous Pxn as the focal adhesion marker for GFP-Vcl and GFP-mVcl and endogenous Vcl for GFP-Pxn and GFP-ePxn.

Rbfox1 expression alters cardiomyoblast morphology and multinucleation

As Rbfox1 expression levels increase during the differentiation process (Figure 1E), we investigated whether Rbfox1 function is directly associated with myoblast differentiation. H9C2 cells were used, as they show cardiac myocyte-like properties under prolonged differentiation conditions (Branco et al., 2015). First, H9C2 cells transfected with empty vector (EV) or RFP-tagged Rbfox1 (Rbfox1-overexpressing) were cultured under normal cell culture conditions. Co-immunostaining of Vcl and actin was performed to independently assess how focal adhesions and the actin cytoskeleton, respectively, were affected. As shown in Figure 5A, considerable changes in focal adhesion structure (Vcl staining) and cytoskeleton organization (actin staining) were readily apparent after 48 h of Rbfox1 transfection. Upon Rbfox1 upregulation, focal adhesion proteins were more concentrated and localized close to the plasma membrane, while in EV-transfected control cells, focal adhesion proteins are more uniformly spread across the cell (Figure 5A). In addition, short actin filaments and ring-shaped structures were observed in Rbfox1-overexpressing cells, accompanied by a significant increase in cellular eccentricity (Figure 5A and B).

The actin cytoskeleton and focal adhesions are key factors for so-called 'primary myoblast fusion', which starts with the activation of a specific myogenic differentiation program. Due to this process, the alignment of myoblasts and myotube membranes as well as the rearrangement of the actin cytoskeleton at contact sites of the plasma membrane is facilitated (Abmayr et al., 2003; Rochlin et al., 2010). Focal adhesions are of particular importance here, as they connect the extracellular matrix with the plasma membrane and the actin cytoskeleton via adaptor proteins (Quach et al., 2009; Samarel, 2014).

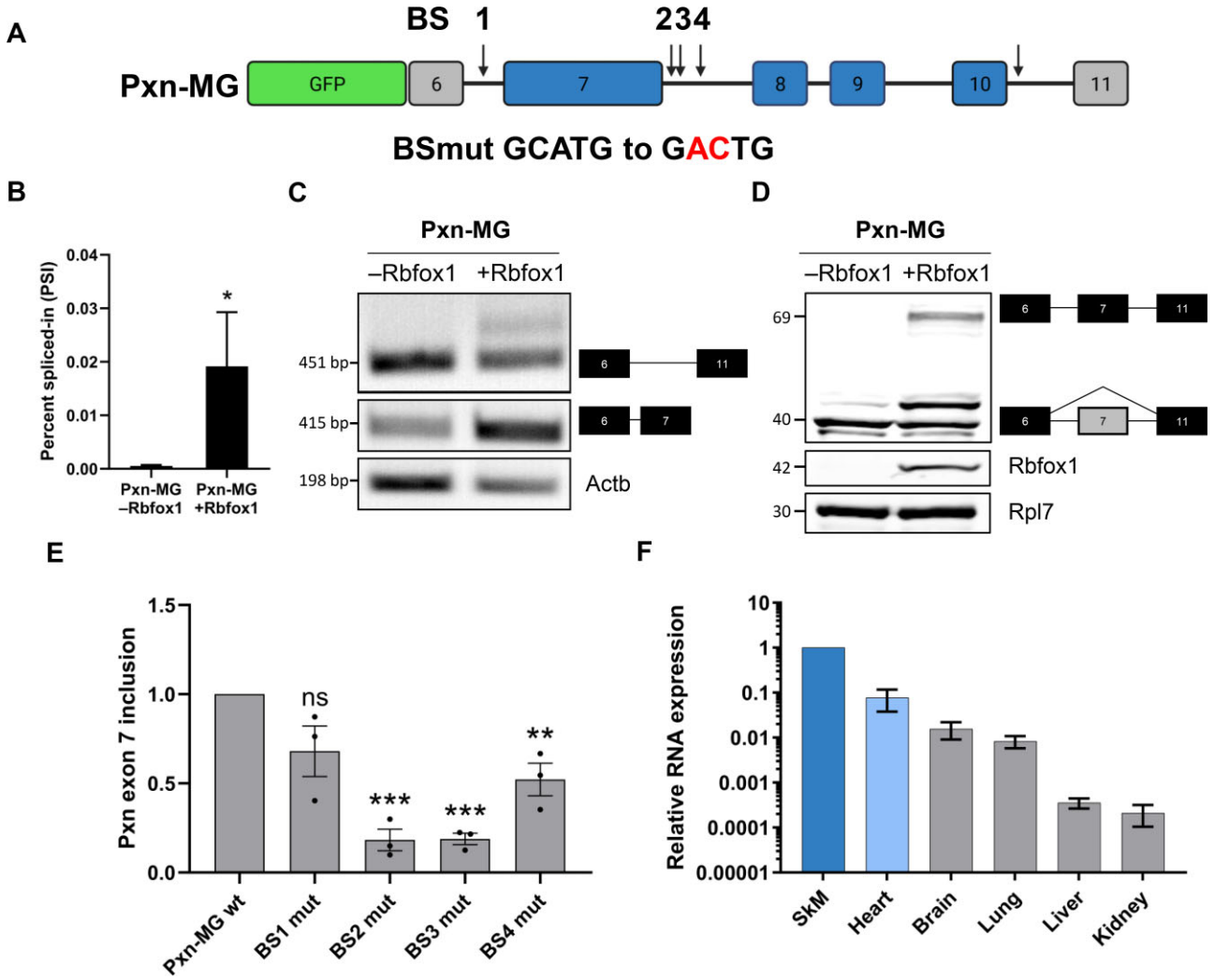

Figure 3 Characterization of the ePxn variant and analysis of the Rbfox1-dependent splicing. (**A**) Minigene construct of Pxn containing GFP followed by exon–intron sequences as displayed; arrows indicate four putative Rbfox1-binding sites with a GCATG motif. For mutational analyses, individual GCATG motifs were mutated to GACTG. (**B**–**D**) Exon 7 inclusion in Pxn-MG was analyzed by RT-qPCR (**B**), semi-quantitative PCR (**C**), and western blotting (**D**). Actb mRNA and Actb protein served as the loading control, respectively. (**E**) Exon 7 inclusion in wild-type Pxn-MG and mutant minigenes harboring single point mutation within the indicated putative Rbfox1-binding site upon Rbfox1 overexpression was determined by RT-qPCR. Shown are the fold changes relative to the wild-type minigene. (**F**) Relative mRNA expression levels of ePxn in various mouse tissues were determined by RT-qPCR. $n = 3$, significance determined by Student's *t*-test. ns, not significant; $^{*}P < 0.05$; $^{**}P < 0.01$; $^{***}P < 0.001$.

Then, H9C2 cells transfected with control siRNA (siC) or a pool of Rbfox1 siRNAs (siRbfox1) were cultured under differentiation conditions. H9C2 cells can use their myogenic potential to differentiate from mononucleated myoblasts to multinucleated myofibers when cultured with retinoic acid (RA) in serum-deprived media (Menard et al., 1999). In conjunction with this, both skeletal and cardiac muscle tissues contain a high percentage of multinucleated cells, although it is more pronounced for the skeletal muscle (Landim-Vieira et al., 2020).

Under normal cardiomyocyte differentiation conditions, H9C2 cells showed clear multinucleation (Figure 5C, left panel). However, when Rbfox1 was depleted, both differentiation progression and the number of multinucleated cells were reduced (Figure 5C, right panel). Quantification of the fraction of multinucleated cells in several optical fields revealed a significant reduction in multinucleated cells following Rbfox1 depletion (Figure 5D). To determine whether Rbfox1 depletion solely alters multinucleation or the differentiation process itself, we analyzed the RNA expression levels of important myogenic differentiation markers in H9C2 cells. Upon Rbfox1 depletion, two myogenic factors Tnnt2 and MyoD were slightly deregulated, whereas Myog remained unaffected (Figure 5E). Meanwhile, the Rbfox1-splicing targets mVcl and ePxn were found profoundly downregulated (Figure 5E). Hence, we assume that the overall

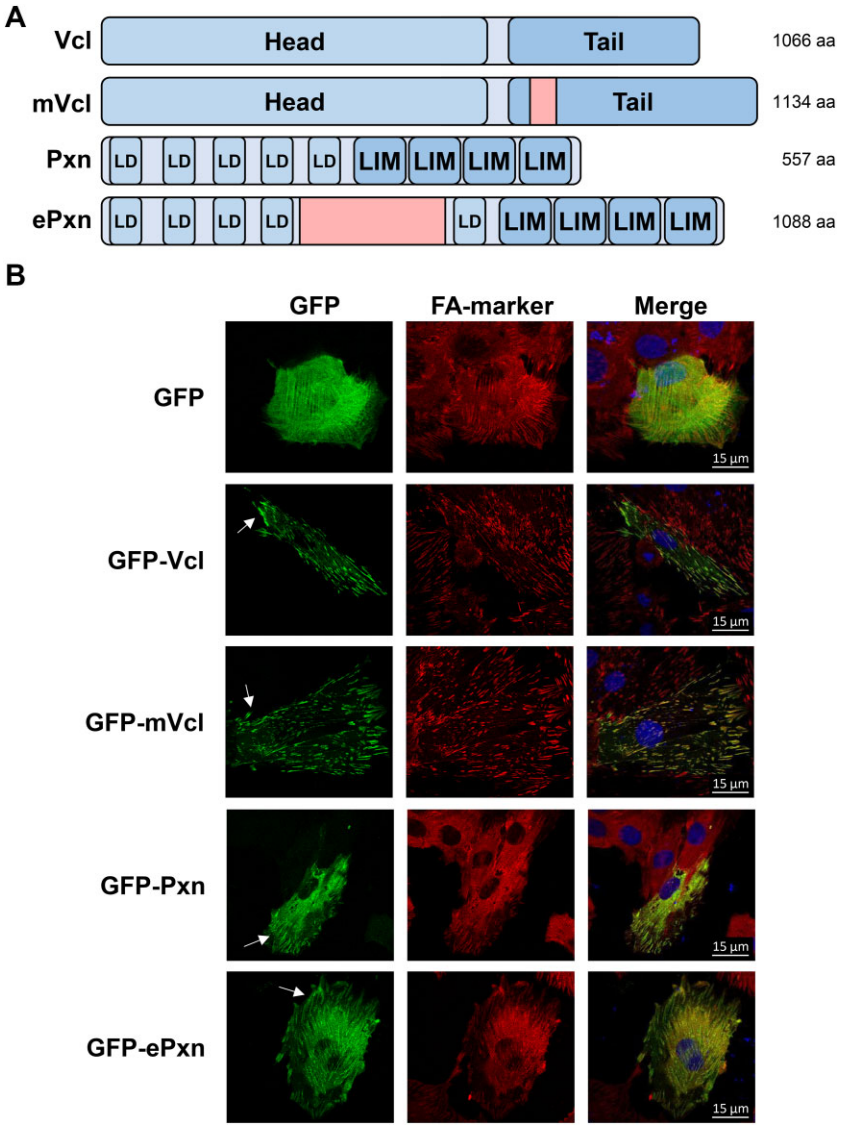

Figure 4 Cellular localization of mVcl and ePxn variants. (**A**) Summary of the protein variants analyzed in this study. The additional exons in ePxn as well as mVcl are depicted in red. Structural features of each protein are highlighted, including leucine and aspartic acid rich (LD) motifs, LIN-11, Isl-1 and MEC-3 (LIM) domains, and head and tail domains. (**B**) H9C2 cells were transfected with GFP, GFP-Vcl, GFP-mVcl, GFP-Pxn, and GFP-ePxn plasmids. Protein localization was analyzed by confocal imaging. Endogenous Pxn was co-stained to indicate focal adhesion complexes for GFP-Vcl and GFP-mVcl transfections, while endogenous Vcl was co-stained for GFP, GFP-Pxn, and GFP-ePxn transfections. Arrows indicate focal adhesion sites. FA-marker, focal adhesion marker. Scale bar, 15 µm.

H9C2 differentiation program might be slightly altered by Rbfox1 depletion and multinucleation is likely connected to Rbfox1-mediated alternative splicing.

Discussion

Alternative splicing is recognized as an important posttranscriptional process that greatly contributes to transcriptome and proteome complexity. The relevance of RNA splicing in cardiac development and disease has recently gained attention with the advent of high-throughput approaches and novel bioinformatic tools (Hasimbegovic et al., 2021). Physiological changes during heart development require an extensive and tightly regulated network of intrinsic splicing factors. Alternative splicing has been demonstrated to play crucial roles in cardiac development and pathologies such as MI (Kalsotra et al., 2008; Giudice et al., 2014; Wang et al., 2016). Genome-wide analyses in compromised hearts provided compelling evidence that subsets of functionally relevant genes are mis-spliced due to downregulation of important splicing factors such as Rbfox1, Rbm20, and SRSF10 (Feng et al., 2009; Guo et al., 2012; Frese et al., 2015; Gao et al., 2016). Worth mentioning is the pivotal role of Rbfox1 in cardiac and skeletal muscle development. Rbfox1 depletion

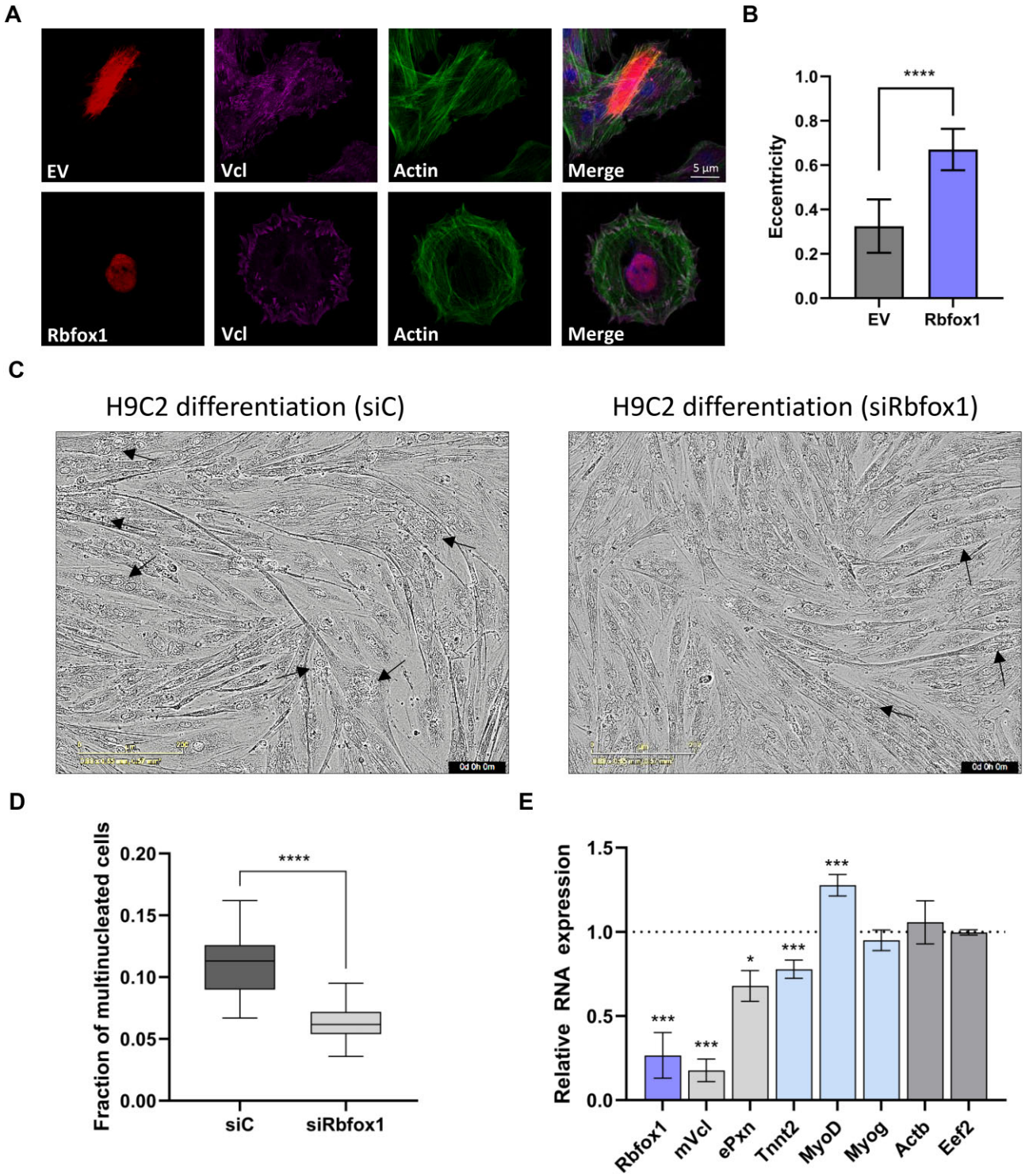

Figure 5 Cellular role of Rbfox1 in cardiomyocyte morphology and differentiation. (**A**) Immunofluorescence analysis of RFP (EV, upper panel) and RFP-tagged Rbfox1 (Rbfox1, lower panel) in H9C2 cells. Endogenous Vcl was co-stained for focal adhesion complexes and is indicated in magenta. Actin is labelled in green, and nuclear DAPI staining is labelled in blue. Scale bar, 5 µm. (**B**) Cellular eccentricity of H9C2 cells quantified from (**A**) using ImageJ software ($n = 15$). (**C**) Microscopy images of differentiated H9C2 cells transfected with siC or siRbfox1 after 6 days of differentiation. Arrows indicate multinucleated cells. (**D**) Quantification of the fraction of multinucleated cells from (**C**) indicates reduced multinucleated cells upon Rbfox1 depletion. (**E**) Relative mRNA expression levels of Rbfox1 splicing targets (mVcl and ePxn), myogenic differentiation markers (Tnnt2, MyoD, and Myog), and control genes (Actb and Eef2) in differentiated H9C2 cells transfected with siRbfox1 vs. siC ($n = 3$). Significance determined by Student's *t*-test. *$P < 0.05$; ***$P < 0.001$; ****$P < 0.0001$.

during cardiac hypertrophy was shown to result in an abnormal splicing pattern in mouse heart and other animal models (Frese et al., 2015; Gao et al., 2016).

In the present study, we corroborated previous findings that showed significant Rbfox1 downregulation in heart failure and cardiac hypertrophy models. Here, we identified an enrichment of Rbfox1-binding sites in intronic regions of focal adhesion genes. Focal adhesions are essential biological structures involved in myoblast cell fusion and controlling force propagation to maintain proper cardiac muscle function (McCain et al., 2012; Samarel, 2014). Therefore, we addressed the question of whether the *in silico* predicted Rbfox1 splicing targets include focal adhesion genes (Figure 1). Cellular function of focal adhesion genes has been thoroughly investigated in the muscle context. In particular, Pxn, Vcl, and Actn1 and their alternatively spliced isoforms were described to be important for muscle cell function (Foley and Young, 2013; Kanoldt et al., 2020). Rbfox1 expression is increased during the differentiation process from myoblasts to myotubes in skeletal and cardiac muscle cells, and Rbfox1-binding sites are enriched in introns of developmentally regulated and alternatively spliced genes in the heart (Kalsotra et al., 2008). Our results confirm that upon skeletal and cardiac differentiation of myoblasts, an uncharacterized Pxn variant (ePxn) and mVcl show concomitant upregulation with Rbfox1.

mVcl and its functions have been described before. It structurally differs from Vcl in its larger tail domain caused by exon 19 inclusion. In contrast to the ubiquitous expression of Vcl, mVcl expression is restricted to cardiac, skeletal, and smooth muscle cells (Feramisco et al., 1982; Belkin et al., 1988; Kim et al., 2016). These findings are in line with our results that show mVcl expression mostly in the skeletal and heart muscle tissues of mice. Additionally, we determined that Rbfox1 regulates alternative splicing of the exon 19 of Vcl, presumably by association with the upstream and downstream binding sites. It was previously reported that Rbfox1-regulated introns often contain multiple binding sites, which was also a criterion for our *in silico* prediction (Figure 1; Conboy, 2017). Hence, we assume that Rbfox1 can also cooperatively regulate its target exons depending on the occurrence of binding sites.

The previously uncharacterized Pxn isoform ePxn was identified in this study to be regulated by Rbfox1. Although ePxn is substantially larger than Pxn, it is still located in focal adhesions (Figure 4B). This infers that the alternatively spliced exons that translate to a highly disordered protein region could have a large regulatory potential for focal adhesions (Supplementary Figure S1B). Intrinsically disordered proteins have gained substantial interest in the past few years; although they lack a stable tertiary structure, their unstructured segments confer a wide variety of biological functions (Uversky et al., 2000; Dunker et al., 2001; Piersimoni et al., 2022). The N-terminus of canonical Pxn has been studied because it includes large and flexible IDRs between the short functional LD motifs, which mostly interact with FAK, Vcl, and Src proteins (Brown et al., 2005; Hu et al., 2014). Such IDRs are becoming recognized as sites of phosphorylation that dynamically modify the interactions within focal adhesions. For instance, tissue-specific alternative splicing of FAK produces additional exons with crucial phosphorylation sites that allow binding of Src family kinases and activation of signal transduction pathways (Toutant et al., 2002). Pxn is among the most connected proteins in focal adhesions and is involved in the recruitment of adaptor proteins for the assembly of the adhesion complex (Brown and Turner, 2004; Brown et al., 2005). In regards to ePxn, we predicted several putative kinase and SH3-domain binding motifs within the alternative exons (Supplementary Figure S1C). We hypothesize that ePxn shows profound post-translational modification patterns and interactions that might influence focal adhesion kinetics and/or assembly.

Overall, differential alternative splicing due to Rbfox1 upregulation might also explain the altered myoblast cell morphology where focal adhesions and the actin cytoskeleton are altered (Figure 5A). mVcl has been shown to alter the binding and flexibility of actin filaments and tune filament organization in the presence of Vcl (Tolbert et al., 2013; Oztug Durer et al., 2015). The cytoskeletal rearrangement could be due to the ability of mVcl and ePxn to engage different binding partners compared to Vcl and Pxn, respectively. We cannot rule out that additional Rbfox1 targets might contribute to the reorganization of the cytoskeleton. In this study, we also identified additional putative Rbfox1 targets that might have a substantial impact on focal adhesions and could also affect Rbfox1-mediated morphological changes (Figure 1D and F). To understand the function of Rbfox1 in cardiac muscle cell differentiation, we utilized an Rbfox1 knockdown and differentiation protocol in H9C2 cells. We observed that Rbfox1 depletion led to the reduced multinucleation, indicating a perturbed differentiation outcome. In addition, we detected mild yet significant differences in the expression levels of myogenic transcription factors following Rbfox1 depletion. Hence, we hypothesize that the differentiation of H9C2 cells can be initiated upon Rbfox1 depletion but is altered at later stages where multinucleation occurs. This includes changes in alternative splicing of focal adhesion genes (e.g. mVcl and ePxn), which might influence not only focal adhesions but also the differentiation process itself. Similar effects (disturbed multinucleation with unaffected myogenic differentiation program) were previously observed by inhibiting FAK, a putative Rbfox1 target (Figure 1F). This highlights that focal adhesion signaling plays an important role in myoblast cell fusion (Quach et al., 2009). Taken together, our findings imply that the splicing factor Rbfox1 is potentially able to promote fusion-competent myoblasts by altering splicing patterns of focal adhesion genes.

Materials and methods

Cell culture, transfection, and differentiation

H9C2 and C2C12 cells were obtained from the American Type Culture Collection (ATCC) and cultured in Dulbecco's modified Eagle's medium (DMEM) and GlutaMAX (Life Technologies) with 20% or 10% fetal bovine serum (FBS; PanBiotech, P30-3031),

respectively. C2C12 cells were used when high transfection efficiency and cell number were needed. For plasmid transfection, C2C12 cells were seeded at a density of 1.5×10^5–2.0×10^5 and transfected using Viromer Red (Lipocalyx) according to the manufacturer's protocol. H9C2 cells were cultivated at 60%–70% confluence to maintain differentiation potential and prevent differentiation during cultivation. Overexpression of plasmid DNA was facilitated by seeding 1.0×10^5–1.5×10^5 H9C2 cells per well in a 6-well plate and using Viromer Yellow (Lipocalyx) according to the manufacturer's protocol (OriGene, manual 01/2016). Knockdown experiments were conducted with similar cell densities using siC and a pool of siRNAs designed to target both mouse and rat Rbfox1 (Supplementary Table S1) with Viromer Blue (Lipocalyx) according to the manufacturer's protocol.

Differentiation experiments were conducted by culturing H9C2 cells (1.0×10^5–1.5×10^5 per well in a 6-well plate at 60%–70% confluency) in DMEM containing 1% FBS for muscle-cell-like differentiation or containing 1% FBS and 2 μM RA (Sigma-Aldrich) for cardiac cell differentiation. Over the course of 7 days, the medium was exchanged every other day and RA was supplied daily.

For the analysis of multinucleation, H9C2 cells were transfected with siC or siRNAs targeting Rbfox1 and subjected to the differentiation process. Cells were fixed with 4% formaldehyde solution and permeabilized with 0.5% Triton-X in phosphate-buffered saline (PBS) for better visualization of nuclei. Images were taken using an IncuCyte S3 (Sartorius) live cell analysis instrument. For each condition, 25 images on the same position of the well were taken. One image was randomly picked for each replicate and condition as a representative image, and total cells (based on nuclei) were manually counted for the average cell number per image. Afterwards, 4 out of the remaining 24 images were randomly chosen, and multinucleated cells were counted manually. The percentage of multinucleated cells was calculated for all images based on the average total cell number per image.

Western blotting

H9C2 and C2C12 cells were transfected with the indicated constructs. After 48 h, the cells were harvested and lysed in total lysis buffer [50 mM Tris, pH 7.4, 50 mM NaCl, 1% sodium dodecyl sulfate (SDS), and 2 mM $MgCl_2$] containing TurboNuclease (Jena Bioscience) for DNA digestion. Protein concentration was measured using the BCA Protein Assay Kit (Bio-Rad), and samples were supplemented with 4× NuPAGE™ LDS Sample Buffer (Invitrogen) and ran on a 4%–12% Bis-Tris SDS Gel using the NuPAGE Invitrogen SDS-Gel system. Gels were blotted on a nitrocellulose membrane using NuPAGE standard protocols from Invitrogen. Following antibody incubation, blots were analyzed by near-infrared scanning (Odyssey scanner, Li-COR) using IRDye680RD/800CW-linked secondary antibodies (Li-COR). The primary antibodies used are listed in Supplementary Table S1.

RNA isolation, semi-quantitative PCR, and RT-qPCR

Total RNA was isolated using TRIzol extraction from H9C2 and C2C12 cells after transfection. cDNA synthesis was performed with random hexamer primers using M-MLV Reverse Transcriptase reagents and protocol (Promega). Semi-quantitative PCR was performed using OneTaq® 2X Master Mix with Standard Buffer (NEB) and 40 PCR cycles. RT-qPCR was performed with ORA qPCR Green ROX L Mix (HighQu) on a LightCycler 480 II (384-well) system (Roche) or with GoTaq® qPCR Mix (Promega) on an MyiQ (96-well) system (Bio-Rad). The PSI value was calculated as the ratio of alternative variants to all variants. For a complete list of primers used, see Supplementary Table S1.

Cloning

The Rbfox1 insert for overexpression plasmids was generated from mouse heart cDNA using the indicated oligonucleotides and subcloned into the vectors as listed in Supplementary Table S1. The Vcl-MG construct was created by sequential insertion of two amplicons into a pcDNA3.1 Flag RFP vector and subcloned into the pEGFP-C1 vector using *Bam*HI/*Not* and *Bam*HI/*Psp*OMI restriction enzymes and T4 DNA Ligase (New England Biolabs). The Pxn-MG construct was created by sequential insertion of two PCR fragments into the pEGFP-C1 vector and subcloned into the pEGFP-C2 vector. To generate minigene point mutants, we purchased DNA fragments containing the desired mutation (GenScript) and replaced in the wild-type construct. Purified DNA from mouse heart was used as a template for minigene cloning with the PureLink Genomic DNA Mini Kit (Invitrogen). All sequences were verified by Sanger sequencing at Eurofins Genomics.

Computational analysis and databases

Rbfox1 RNA expression data were extracted from publicly available sequencing data of the EGFR-KO mouse model (Schreier et al., 2013) as well as TAC and MI mouse models (GSE96561). Mean values of relative expression and standard deviation were calculated from individual fragments per kilobase per million mapped fragments (FPKM) values of the respective mouse samples. For the analysis of putative Rbfox1-binding motifs in the mouse genome and heart genes, intron sequences of the whole mouse genome were accessed via the Ensembl Biomart tool. Intronic sequences were blasted for Rbfox1-binding sites (TGCATG and GCATG) utilizing the Basic Local Alignment Search Tool (BLAST+ desktop application) as previously described (Zorn et al., 2021). For further analysis, the reported binding sites were listed as the total number of binding sites in all introns of a specific gene. Heart-specific genes containing Rbfox1-binding sites were evaluated through comparison of the whole-genome gene list with genes expressed in mouse heart according to the RNA-seq dataset E-MTAB-3725. An arbitrary threshold of 10 transcripts per million mapped fragments was used to obtain a more reliable list of robustly expressed transcripts. Additionally, a cutoff of at least 20 putative Rbfox1-binding sites was chosen for a more representative

gene set. Genes with <20 putative binding sites could still be regulated by Rbfox1 but were not considered for our initial investigation. Although non-coding RNAs were also reported in the BLAST analysis, they were discarded from this study. The full gene list is shown in Supplementary Table S2. These genes were uploaded to the DAVID bioinformatics database (Sherman et al., 2022) and processed in the functional annotation tool to sort them into functional clusters. Molecular weights of the alternatively spliced variants and the kinase recognition motifs were extracted from HPRD. Prediction of the protein structure of ePxn was performed with the AlphaFold Protein Structure Database, and the structure model was visualized using PyMOL.

Immunostaining

Cells were transfected and, after 24 h, were seeded on coverslips in a 24-well plate and cultured overnight. Then, the cells were washed using PBS and fixed with 4% formaldehyde solution, followed by permeabilization with 0.5% Triton-X and blocking with 2% bovine serum albumin (BSA) in PBS. The samples were incubated with primary antibodies for Vcl and Pxn (1:1000 in 2% BSA in PBS) for 1 h at room temperature and then with Cy3- and AlexaFluor488-conjugated secondary antibodies (Dianova). Overexpression of Pxn, ePxn, Vcl, and mVcl was detected based on the fluorescence of GFP fusion proteins. Actin staining was performed using Phalloidin-iFluor 488 Reagent according to the manufacturer's instructions (Abcam). Images were acquired on a Leica LSM SP5X confocal microscope using a 63× oil objective and Leica imaging software.

Supplementary material

Supplementary material is available at *Journal of Molecular Cell Biology* online.

Acknowledgements

We especially thank the team of the Core Facility Imaging, Medical Faculty, Martin-Luther-University Halle–Wittenberg for assistance with image acquisition and analysis. Figures 1D, 2A, and 3A were created with BioRender.com licensed to M.K.

Funding

This work was supported by grants from the Deutsche Forschungsgemeinschaft [DFG, German Research Foundation; RTG 2467, project number 391498659 'Intrinsically disordered proteins—molecular principles, cellular functions, and diseases'; FOR 5433, project number 468534282 'RNA in focus (RIF): from mechanisms to novel therapeutic strategies in cancer treatment'] and the Wilhelm-Roux-Program (Medical Faculty, Martin-Luther-University Halle–Wittenberg).

Conflict of interest: none declared.

References

Abmayr, S.M., Balagopalan, L., Galletta, B.J., et al. (2003). Cell and molecular biology of myoblast fusion. Int. Rev. Cytol. *225*, 33–89.

Amrani, Y., and Panettieri, R.A. (2003). Airway smooth muscle: contraction and beyond. Int. J. Biochem. Cell Biol. *35*, 272–276.

Baralle, F.E., and Giudice, J. (2017). Alternative splicing as a regulator of development and tissue identity. Nat. Rev. Mol. Cell Biol. *18*, 437–451.

Belkin, A.M., Ornatsky, O.I., Kabakov, A.E., et al. (1988). Diversity of vinculin/meta-vinculin in human tissues and cultivated cells. Expression of muscle specific variants of vinculin in human aorta smooth muscle cells. J. Biol. Chem. *263*, 6631–6635.

Binas, S., Knyrim, M., Hupfeld, J., et al. (2020). miR-221 and -222 target CACNA1C and KCNJ5 leading to altered cardiac ion channel expression and current density. Cell. Mol. Life Sci. *77*, 903–918.

Boutz, P.L., Stoilov, P., Li, Q., et al. (2007). A post-transcriptional regulatory switch in polypyrimidine tract-binding proteins reprograms alternative splicing in developing neurons. Genes Dev. *21*, 1636–1652.

Branco, A.F., Pereira, S.P., Gonzalez, S., et al. (2015). Gene expression profiling of H9c2 myoblast differentiation towards a cardiac-like phenotype. PLoS One *10*, e0129303.

Brown, M.C., Cary, L.A., Jamieson, J.S., et al. (2005). Src and FAK kinases cooperate to phosphorylate paxillin kinase linker, stimulate its focal adhesion localization, and regulate cell spreading and protrusiveness. Mol. Biol. Cell *16*, 4316–4328.

Brown, M.C., and Turner, C.E. (2004). Paxillin: adapting to change. Physiol. Rev. *84*, 1315–1339.

Cestra, G., Castagnoli, L., Dente, L., et al. (1999). The SH3 domains of endophilin and amphiphysin bind to the proline-rich region of synaptojanin 1 at distinct sites that display an unconventional binding specificity. J. Biol. Chem. *274*, 32001–32007.

Conboy, J.G. (2017). Developmental regulation of RNA processing by Rbfox proteins. Wiley Interdiscip. Rev. RNA *8*, 10.1002/wrna.1398.

Damianov, A., and Black, D.L. (2010). Autoregulation of Fox protein expression to produce dominant negative splicing factors. RNA *16*, 405–416.

Duan, Q., McMahon, S., Anand, P., et al. (2017). BET bromodomain inhibition suppresses innate inflammatory and profibrotic transcriptional networks in heart failure. Sci. Transl. Med. *9*, eaah5084.

Dunker, A.K., Lawson, J.D., Brown, C.J., et al. (2001). Intrinsically disordered protein. J. Mol. Graph. Model. *19*, 26–59.

Feng, Y., Valley, M.T., Lazar, J., et al. (2009). SRp38 regulates alternative splicing and is required for Ca^{2+} handling in the embryonic heart. Dev. Cell *16*, 528–538.

Feramisco, J.R., Smart, J.E., Burridge, K., et al. (1982). Co-existence of vinculin and a vinculin-like protein of higher molecular weight in smooth muscle. J. Biol. Chem. *257*, 11024–11031.

Foley, K.S., and Young, P.W. (2013). An analysis of splicing, actin-binding properties, heterodimerization and molecular interactions of the non-muscle α-actinins. Biochem. J. *452*, 477–488.

Frese, K.S., Meder, B., Keller, A., et al. (2015). RNA splicing regulated by RBFOX1 is essential for cardiac function in zebrafish. J. Cell Sci. *128*, 3030–3040.

Gao, C., Ren, S., Lee, J.H., et al. (2016). RBFox1-mediated RNA splicing regulates cardiac hypertrophy and heart failure. J. Clin. Invest. *126*, 195–206.

Giudice, J., Xia, Z., Wang, E.T., et al. (2014). Alternative splicing regulates vesicular trafficking genes in cardiomyocytes during postnatal heart development. Nat. Commun. *5*, 3603.

Gunawan, F., Gentile, A., Fukuda, R., et al. (2019). Focal adhesions are essential to drive zebrafish heart valve morphogenesis. J. Cell Biol. *218*, 1039–1054.

Guo, W., Schafer, S., Greaser, M.L., et al. (2012). RBM20, a gene for hereditary cardiomyopathy, regulates titin splicing. Nat. Med. *18*, 766–773.

Hasimbegovic, E., Schweiger, V., Kastner, N., et al. (2021). Alternative splicing in cardiovascular disease—a survey of recent findings. Genes *12*, 1457.

Hirth, S., Buhler, A., Buhrdel, J.B., et al. (2016). Paxillin and focal adhesion kinase (FAK) regulate cardiac contractility in the zebrafish heart. PLoS One *11*, e0150323.

Hu, Y.L., Lu, S., Szeto, K.W., et al. (2014). FAK and paxillin dynamics at focal adhesions in the protrusions of migrating cells. Sci. Rep. *4*, 6024.

Jin, Y., Suzuki, H., Maegawa, S., et al. (2003). A vertebrate RNA-binding protein Fox-1 regulates tissue-specific splicing via the pentanucleotide GCAUG. EMBO J. *22*, 905–912.
Jumper, J., Evans, R., Pritzel, A., et al. (2021). Highly accurate protein structure prediction with AlphaFold. Nature *596*, 583–589.
Kalsotra, A., Xiao, X., Ward, A.J., et al. (2008). A postnatal switch of CELF and MBNL proteins reprograms alternative splicing in the developing heart. Proc. Natl Acad. Sci. USA *105*, 20333–20338.
Kanoldt, V., Kluger, C., Barz, C., et al. (2020). Metavinculin modulates force transduction in cell adhesion sites. Nat. Commun. *11*, 6403.
Kim, L.Y., Thompson, P.M., Lee, H.T., et al. (2016). The structural basis of actin organization by vinculin and metavinculin. J. Mol. Biol. *428*, 10–25.
Klinck, R., Fourrier, A., Thibault, P., et al. (2014). RBFOX1 cooperates with MBNL1 to control splicing in muscle, including events altered in myotonic dystrophy type 1. PLoS One *9*, e107324.
Kuroyanagi, H. (2009). Fox-1 family of RNA-binding proteins. Cell. Mol. Life Sci. *66*, 3895–3907.
Lambert, N., Robertson, A., Jangi, M., et al. (2014). RNA Bind-n-seq: quantitative assessment of the sequence and structural binding specificity of RNA binding proteins. Mol. Cell *54*, 887–900.
Landim-Vieira, M., Schipper, J.M., Pinto, J.R., et al. (2020). Cardiomyocyte nuclearity and ploidy: when is double trouble? J. Muscle Res. Cell Motil. *41*, 329–340.
Maeda, M., Holder, E., Lowes, B., et al. (1997). Dilated cardiomyopathy associated with deficiency of the cytoskeletal protein metavinculin. Circulation *95*, 17–20.
McCain, M.L., Lee, H., Aratyn-Schaus, Y., et al. (2012). Cooperative coupling of cell–matrix and cell–cell adhesions in cardiac muscle. Proc. Natl Acad. Sci. USA *109*, 9881–9886.
Menard, C., Pupier, S., Mornet, D., et al. (1999). Modulation of L-type calcium channel expression during retinoic acid-induced differentiation of H9C2 cardiac cells. J. Biol. Chem. *274*, 29063–29070.
Minovitsky, S., Gee, S.L., Schokrpur, S., et al. (2005). The splicing regulatory element, UGCAUG, is phylogenetically and spatially conserved in introns that flank tissue-specific alternative exons. Nucleic Acids Res. *33*, 714–724.
Nakahata, S., and Kawamoto, S. (2005). Tissue-dependent isoforms of mammalian Fox-1 homologs are associated with tissue-specific splicing activities. Nucleic Acids Res. *33*, 2078–2089.
Neerathilingam, M., Bairy, S.G., and Mysore, S. (2016). Deciphering mode of action of functionally important regions in the intrinsically disordered paxillin (residues 1–313) using its interaction with FAT (focal adhesion targeting domain of focal adhesion kinase). PLoS One *11*, e0150153.
Oztug Durer, Z.A., McGillivary, R.M., Kang, H., et al. (2015). Metavinculin tunes the flexibility and the architecture of vinculin-induced bundles of actin filaments. J. Mol. Biol. *427*, 2782–2798.
Park, J.Y., Li, W., Zheng, D., et al. (2011). Comparative analysis of mRNA isoform expression in cardiac hypertrophy and development reveals multiple post-transcriptional regulatory modules. PLoS One *6*, e22391.
Pedrotti, S., Giudice, J., Dagnino-Acosta, A., et al. (2015). The RNA-binding protein Rbfox1 regulates splicing required for skeletal muscle structure and function. Hum. Mol. Genet. *24*, 2360–2374.
Piersimoni, L., Abd El Malek, M., Bhatia, T., et al. (2022). Lighting up Nobel Prize-winning studies with protein intrinsic disorder. Cell. Mol. Life Sci. *79*, 449.
Quach, N.L., Biressi, S., Reichardt, L.F., et al. (2009). Focal adhesion kinase signaling regulates the expression of caveolin 3 and β1 integrin, genes essential for normal myoblast fusion. Mol. Biol. Cell *20*, 3422–3435.
Rochlin, K., Yu, S., Roy, S., et al. (2010). Myoblast fusion: when it takes more to make one. Dev. Biol. *341*, 66–83.
Samarel, A.M. (2014). Focal adhesion signaling in heart failure. Pflugers Arch. *466*, 1101–1111.
Schreier, B., Rabe, S., Schneider, B., et al. (2013). Loss of epidermal growth factor receptor in vascular smooth muscle cells and cardiomyocytes causes arterial hypotension and cardiac hypertrophy. Hypertension *61*, 333–340.
Sherman, B.T., Hao, M., Qiu, J., et al. (2022). DAVID: a web server for functional enrichment analysis and functional annotation of gene lists (2021 update). Nucleic Acids Res. *50*, W216–W221.
Siliciano, J.D., and Craig, S.W. (1982). Meta-vinculin—a vinculin-related protein with solubility properties of a membrane protein. Nature *300*, 533–535.
Tapial, J., Ha, K.C.H., Sterne-Weiler, T., et al. (2017). An atlas of alternative splicing profiles and functional associations reveals new regulatory programs and genes that simultaneously express multiple major isoforms. Genome Res. *27*, 1759–1768.
Tolbert, C.E., Burridge, K., and Campbell, S.L. (2013). Vinculin regulation of F-actin bundle formation: what does it mean for the cell? Cell Adh. Migr. *7*, 219–225.
Toutant, M., Costa, A., Studler, J.M., et al. (2002). Alternative splicing controls the mechanisms of FAK autophosphorylation. Mol. Cell. Biol. *22*, 7731–7743.
Uversky, V.N., Gillespie, J.R., and Fink, A.L. (2000). Why are 'natively unfolded' proteins unstructured under physiologic conditions? Proteins *41*, 415–427.
Varadi, M., Anyango, S., Deshpande, M., et al. (2022). AlphaFold Protein Structure Database: massively expanding the structural coverage of protein-sequence space with high-accuracy models. Nucleic Acids Res. *50*, D439–D444.
Wang, H., Chen, Y., Li, X., et al. (2016). Genome-wide analysis of alternative splicing during human heart development. Sci. Rep. *6*, 35520.
Weyn-Vanhentenryck, S.M., Feng, H., Ustianenko, D., et al. (2018). Precise temporal regulation of alternative splicing during neural development. Nat. Commun. *9*, 2189.
Zemljic-Harpf, A.E., Miller, J.C., Henderson, S.A., et al. (2007). Cardiac-myocyte-specific excision of the vinculin gene disrupts cellular junctions, causing sudden death or dilated cardiomyopathy. Mol. Cell. Biol. *27*, 7522–7537.
Zhang, C., Frias, M.A., Mele, A., et al. (2010). Integrative modeling defines the Nova splicing-regulatory network and its combinatorial controls. Science *329*, 439–443.
Zhang, C., Zhang, Z., Castle, J., et al. (2008). Defining the regulatory network of the tissue-specific splicing factors Fox-1 and Fox-2. Genes Dev. *22*, 2550–2563.
Zorn, P., Misiak, D., Gekle, M., et al. (2021). Identification and initial characterization of POLIII-driven transcripts by msRNA-sequencing. RNA Biol. *18*, 1807–1817.

Received April 5, 2023. Revised November 30, 2023. Accepted January 19, 2024.